PNAS
www.pnas.org

Main Manuscript for

On the Effects of the Ocean on Atmospheric CFC-11 Lifetimes And Emissions

Peidong Wang[a], Jeffery R. Scott[a], Susan Solomon[a], John Marshall[a], Andrew R. Babbin[a], Megan Lickley[a], David W. J. Thompson[b], Timothy DeVries[c], Qing Liang[d], Ronald G. Prinn[a]

[a]Earth, Atmospheric, and Planetary Sciences, Massachusetts Institute of Technology, Cambridge, MA 02139; [b]Department of Atmospheric Science, Colorado State University, Fort Collins, CO 80523; [c]Department of Geography, University of California, Santa Barbara, CA 93106; [d]Atmospheric Chemistry and Dynamics Laboratory, NASA Goddard Space Flight Center, Greenbelt, MD 20771

*Peidong Wang

Email: pdwang@mit.edu

Author Contributions: S.S., P.W., J.R.S., D.W.J.T. and T.D. conceptualized the work; J.R.S. contributed the model setup; P.W. conducted the analysis; P.W. and S.S. drafted the manuscript; and all authors revised the paper.

Competing Interest Statement: The authors declare no conflict of interest.

Classification: Physical Sciences – Earth, Atmospheric, and Planetary Sciences

Keywords: CFC-11; air-sea flux; lifetime estimates; emission estimates

This PDF file includes:

Abstract

The ocean is a reservoir for CFC-11, a major ozone-depleting chemical. Anthropogenic production of CFC-11 dramatically decreased in the 1990s under the Montreal Protocol, which stipulated a global phase-out of production by 2010. However, studies raise questions about current overall emission levels, and indicate unexpected increases of CFC-11 emissions of about 10 Gg yr^{-1} after 2013 (based upon measured atmospheric concentrations and an assumed atmospheric lifetime). These findings heighten the need to understand processes that could affect the CFC-11 lifetime, including ocean fluxes. We evaluate for the first time how ocean uptake and release through 2300 affects CFC-11 lifetimes, emission estimates, and the long-term return of CFC-11 from the ocean reservoir. We show that ocean uptake yields a shorter total lifetime and larger inferred emission of atmospheric CFC-11 from 1930 to 2075 compared to estimates using only atmospheric processes. Ocean flux changes over time result in small but not completely negligible effects on the calculated unexpected emissions change (decreasing it by 0.4 ± 0.3 Gg yr^{-1}). Moreover, it is expected that the ocean will eventually become a source of CFC-11, increasing its total lifetime thereafter. Ocean outgassing should produce detectable increases in global atmospheric CFC-11 abundances by the mid-2100s, with emission of around 0.5 Gg yr^{-1}; this should not be confused with illicit production at that time. An illustrative model projection suggests that climate change is expected to make the ocean a weaker reservoir for CFC-11, advancing the detectable change in global atmospheric mixing ratio by about 5 years.

Significance Statement

Manufactured CFC-11 is depleting the Antarctic ozone layer. CFC production has been strictly controlled by the Montreal Protocol, but emission estimates are very sensitive to choices of lifetimes, which are often assumed to be constant over time. We employ a hierarchy of models to study the effect of the ocean on the time-dependent uptake and release of atmospheric CFC-11. The ocean is a sink for CFC-11 and significantly affects its total lifetime and hence the emission inferred from concentration data of past decades. This has not been explicitly included in international ozone assessments. We show that as anthropogenic production ceases, ocean fluxes become more important, suggesting a need for further studies with high-resolution global models linking atmospheric chemistry and ocean processes.

Main Text

Introduction

Man-made chlorofluorocarbons (CFCs) are the primary cause of the Antarctic ozone hole (1). The atmospheric lifetimes of these chemicals range from about 50 – 500 years. The Montreal Protocol agreed to a complete phase out of CFC production and consumption worldwide by 2010. Evidence for healing of the Antarctic ozone layer has indeed emerged (2, 3), indicating the overall success of the Montreal Protocol. Atmospheric loss processes of CFC-11, the most abundant ozone-destroying chlorofluorocarbon, are due to photolysis and reaction with excited oxygen (O^1D) once the gas reaches the stratosphere. The atmospheric lifetime of CFC-11 is assumed to be inversely related to the atmospheric abundance of the molecule, with due consideration of the lag times between tropospheric and stratospheric burdens (4). Given its lifetime of about 50 – 60 years and continued emissions from storage banks such as chillers and building insulation foams (5), the CFC-11 inventory in the atmosphere is decreasing slowly. However, the rate of decrease in atmospheric concentrations has been slowing down since about 2012, suggesting higher overall emission and an unexpected additional post-2013 emission increase of CFC-11 of about 7 – 13 Gg yr^{-1} (10 – 20 % of the total global emission during that time; 6, 7). The latter is clearly inconsistent with the zero global new production that has been agreed by the Montreal Protocol.

CFC-11 is soluble in water, and therefore the ocean has absorbed some CFC-11 from the atmosphere. CFC-11 ocean uptake is greatest in high latitudes where cold sea surface temperatures (SST) enhance CFC-11 solubility (8), and mixing and transport from the surface into the deep ocean is enhanced. By 1994, the ocean had stored up to 1 % of the total anthropogenic emissions of CFC-11 (9), and by 2014 the ocean held roughly 110 Gg of CFC-11 (10), or about 5 – 10 % of the CFC-11 inventory in the various anthropogenic storage banks. While some CFC-11 is removed in sulfidic anoxic waters (11), this effect is small for the current climate, and CFC-11 has long been employed as a useful passive tracer to study ocean circulation (e.g. 12, 13). Early studies using a global model incorporating CFC-11 air-sea fluxes suggested that the ocean's effects on atmospheric CFC-11 lifetimes and concentrations were negligible in the 1980s, when anthropogenic emissions were high (14). However, now that anthropogenic emissions have dramatically decreased and attention is focused on unexpected emissions of 10 Gg or even less, changes in ocean uptake of CFC-11 could be affecting the atmospheric CFC-11 inventory enough to influence emission estimates, and could introduce a time-dependent effect on its total lifetime. Further, as anthropogenic emissions continue to decrease in the future, the ocean must eventually become supersaturated with CFC-11, and turn into a source instead of a sink. No study has yet estimated when that should be expected to occur, and what its magnitude will be.

Here, we address the following questions: (i) How is the ocean affecting the atmospheric CFC-11 inventory, the lifetime of CFC-11 in the atmosphere and its time dependence, and how does this in turn influence emission estimates based on observed concentrations?; (ii) When will the ocean become a source of CFC-11 to the atmosphere, and how much will ocean outgassing affect the apparent emission and atmospheric mixing ratio in the future? (iii) How will climate change affect ocean CFC-11 uptake in the future?

For a conceptual understanding, we use a hierarchy of models starting with a simple 6-box model that simulates the CFC-11 inventory in the atmosphere, ocean mixed layer, and deep ocean layers (each layer has 2 boxes representing the two hemispheres, see the schematic in Figure 1a). CFC-11 in each box is assumed to be well mixed in this illustrative model. The atmospheric CFC-11 lifetime is kept constant at 55 years and estimated emissions are taken from published work (15). We assume constant inter-hemispheric exchange timescales for each layer, and constant cross-layer timescales for mixed layer to deep ocean exchange (see Table S1). Atmospheric CFC-11's vertical distribution does affect its lifetime and surface concentration. Here, we subsume stratosphere-troposphere exchange into our adopted atmospheric lifetime estimates assuming a well-mixed atmosphere, and focus on the ocean's effect on atmospheric CFC-11. We then replace the four ocean boxes with a more sophisticated albeit low-resolution representation of the ocean, the MIT general circulation model (MITgcm; 16, 17), which includes a physics-based CFC-11 air-sea flux and transport into the interior ocean, and treats CFC-11 as a conservative tracer in the ocean (depicted in Figure 1b). The MITgcm (for brevity, we refer to the combined coupled box model atmosphere-ocean model simply as the MITgcm) is run in two modes. First, we use the model forced with climatological average wind stress and buoyancy fluxes (Hist run) to assess the influence of parameters including SST, wind stress, etc. on air-sea CFC-11 fluxes. Second, we force the MITgcm using global monthly RCP8.5 output from the MPI-ESM-LR (Max-Planck-Institute Earth System Model low resolution version) fully coupled global climate model (RCP8.5 run; 18, 19). This model has been shown to provide a realistic response of the Southern Ocean (55 – 70 °S), the region that stores the most CFC-11, to the southern annular mode (20). In the RCP8.5 run, interannual variability within the MPI-ESM-LR output provides changes in the forcing of the ocean applied after 1930, but variability in the atmospheric circulation is not explicitly incorporated into the box model atmosphere. We compare these runs to a "no ocean" run in which the CFC-11 air-sea flux is turned off. Both the box model and MITgcm runs extend from 1930 (essentially the start of emission of this anthropogenic gas) to 2300.

Results

Near-term CFC-11

To evaluate the performance of the box model and MITgcm, we compared the computed CFC-11 atmospheric concentrations with observations (Figure 2a). While the box model is essentially tuned, the MITgcm setup is a fairly standard, off-the-shelf coarse resolution global ocean model without any specific tuning for this application. Both the box model and MITgcm agree well with observations, capturing the increase in CFC-11 before 1990 due to the large anthropogenic emissions, as well as the concentration decrease after 1990 given the decline in the emissions and losses due to chemical reactions in the atmosphere and exchange with CFC-11 depleted ocean waters. The gradient in CFC-11 between the northern hemisphere (NH) and southern hemisphere (SH) is also well captured. Because most of the emissions (around 90%) occur in the NH and the CFC-11 lifetime is long, the NH minus SH difference can be up to 17 ppt when anthropogenic emissions are large (comparable to 20 ppt reported in (21)). As the emissions decrease, the inter-hemispheric exchange brings the NH and SH CFC-11 abundances closer to each other. Both the box model and MITgcm slightly underestimate the observed CFC-11 mixing ratio after 1990, as emissions decline (2.0 ppt lower in box model; 2.7 ppt lower in MITgcm averaged from 1990 to 2017). Reasons for the underestimation of the atmospheric CFC-11 concentration could be either 1) the ocean uptake is overestimated; 2) the CFC-11 atmosphere-only lifetime at that time is larger than our adopted constant value; and/or 3) CFC-11 emissions are higher than those prescribed in this simulation.

Figures 2b and c provide a qualitative comparison of the MITgcm global ocean column-integrated CFC-11 with observations for 1994 (9). The MITgcm captures the spatial distribution of observed CFC-11 in the ocean rather well given a well-mixed atmospheric CFC-11 distribution, indicating that local dynamics is the driving factor for ocean uptake. Intercomparisons between the MITgcm and other models of similar resolution as well as observations (22) also indicate that the MITgcm does a favorable job in simulating CFC-11 distribution. In the MITgcm, CFC-11 is overestimated in the Weddell Sea, although the Weddell Sea only stores less than 4.5 % of the global ocean CFC-11 inventory (not shown) and has only a minor impact on the global estimate (also note (22) showed large model spread in the Southern Ocean inventory due to ventilation differences among models). Most CFC-11 in the NH ocean is stored in the North Atlantic, with subduction into the thermocline and the Atlantic Meridional Overturning Circulation (AMOC) playing key roles (13). The SH is the major reservoir for CFC-11, which is transported in Antarctic Intermediate Water and Subantarctic Mode Water (23) and accumulates in the interior ocean between 40 °S to 60 °S. In 1994, the best estimate of the global ocean CFC-11 inventory from the World Ocean Circulation Experiment (WOCE) is 75.6 Gg (with cumulative error of 16.5 Gg; 9), while the MITgcm suggests about 82 Gg of CFC-11 in the same year, which is slightly larger but well within the uncertainty range of the observational value.

Box model sensitivity tests

For a conceptual understanding of the primary factors affecting CFC-11 inventories in the atmosphere and ocean, we perturbed key parameters (Table S1) in the box model by ± 15 % (Figure S1a). Before 1990, all the sensitivity tests produce similar CFC-11 inventories for both the atmosphere and ocean, underscoring that high anthropogenic emission dominated the behavior during that time. After 1990 as global emissions decrease, the importance of other drivers in affecting CFC-11 inventories increases. For example, a 15 % change in the prescribed atmospheric CFC-11 lifetime affects the atmospheric inventory by up to about 570 Gg in 2050s, or about 15 % of the total atmospheric CFC-11 inventory at that time. A 15 % change in mixed layer depth (MLD; a proxy in the box model for the rate of ventilation of intermediate waters) affects the atmospheric inventory by up to 13 Gg in 1990s. The biggest impact of MLD on CFC-11 inventory is expected to occur in the 20th century because larger CFC-11 emissions and undersaturated ocean waters result in the highest ocean uptake then. Changing the piston velocity only has a small effect on the CFC-11 atmospheric inventory, up to 0.1 Gg. Changes in inter-hemispheric exchange constants adopted for the atmospheric and ocean reservoirs only affect the NH to SH gradient, but do not affect the total inventory in each reservoir, and ± 15 % changes in this parameter only generate differences within computational error. However, in the real world if the exchange timescales between different CFC-11 reservoirs (for example between the atmosphere and ocean, or the atmospheric loss in the stratosphere versus the troposphere) are significantly different in each hemisphere, the effects of inter-hemispheric exchange could become more significant.

The MLD in the box model affects the CFC-11 concentration in the shallow ocean boxes. A deeper MLD implies that the ocean has a larger capacity to store CFC-11. This is crucial to determining whether the ocean is supersaturated or undersaturated with CFC-11 at the air-sea interface. Our box model assumes a constant MLD in time. In the real world and in more complex ocean models, ocean circulation changes can be expected to be dominant factors driving surface ocean CFC-11 concentration, and changes in the meridional overturning circulation with climate change are likely to be important. This highlights the importance of using an ocean model with realistic ocean dynamics to understand CFC-11 evolution in the atmosphere and ocean, as done here with the MITgcm (albeit with low spatial resolution in this configuration of the MITgcm). Figure S1b shows CFC-11 inventories using the MITgcm. Ocean inventories in the box model and MITgcm agree well before 1990 because emission is the driving factor for CFC-11 air-sea fluxes, but they deviate significantly in the future, when ocean dynamics begins to drive changes in surface ocean CFC-11 concentration and the air-sea flux. Our box model only has two ocean layers, which equilibrate CFC-11 between the atmosphere and ocean more rapidly than the MITgcm. Further, some CFC-11 can be transported very deep in the ocean. With 15 ocean layers in the MITgcm, the ocean is able to sequester more CFC-11 in the interior and it takes more time to release that CFC-11 back to the atmosphere, such that the ocean CFC-11 inventory peaks in the year 2075 in the MITgcm, roughly 80 years after the peak in atmospheric CFC-11 concentrations.

Box model results should be considered illustrative rather than quantitative regarding the future CFC-11 inventory. Nonetheless, although some parameters in the box model may have co-dependencies in the real world, our sensitivity analysis qualitatively highlights the importance of two key factors that affect the CFC-11 inventory as anthropogenic emissions drop: the atmospheric lifetime and ocean dynamics. We next focus on the MITgcm results to further explore these issues.

Effect of the ocean on atmospheric CFC-11 concentration

We first present results using the climatological ocean forcing adopted in the Hist scenario. Figure 3a shows the difference in CFC-11 atmospheric inventories and abundances between the MITgcm run and no ocean runs. A similar plot but for dichlorodifluoromethane, or CFC-12, is shown in Figure S2. CFC-11 and CFC-12 are treated in the same manner in the MITgcm but CFC-12 is less soluble; therefore results for CFC-12 generally follow the same pattern as CFC-11 but the magnitude is smaller. Under this forcing, the cumulative effect of the ocean reaches its maximum in 2009, at which point the atmospheric CFC-11 inventory is 76.6 Gg less with the presence of the ocean (equivalent to 3.5 ppt less mole fraction) compared to the no ocean run. As anthropogenic emissions further decrease, the CFC-11 gradient between the atmosphere and the ocean decreases, decreasing the flux going into the ocean. Atmospheric CFC-11 differences between the ocean and no ocean runs reach zero around 2135. After that, the atmosphere accumulates more CFC-11 due to release from the ocean, and this outgassing accumulates in the atmosphere. Based on the current typical detection precision of CFC-11 measurements (24) for the AGAGE (Advanced Global Atmospheric Gases Experiment) network, the net increase of global CFC-11 released from the ocean is expected to become detectable by 2145 or earlier based on this model. At that point, the atmosphere is expected to contain about 0.5 ppt more average CFC-11 compared to a no ocean run (and the global average abundance of CFC-11 is about 50 ppt at that time). Future instrument improvements may allow earlier detection. By 2225, the atmosphere contains about 16 Gg more CFC-11 than in the no ocean run (about 0.8 ppt). The ocean keeps releasing CFC-11 back to the atmosphere until the end of our study period. By the end of the run in 2300, the effect of the ocean on atmospheric CFC-11 remains significant.

The calculated CFC-11 hemispherically integrated air-sea flux is shown in Figure 3b. Most of the uptake in the NH happens in northward-flowing western boundary currents of the North Atlantic and North Pacific (Figure S3a-d), due to local cooling and the upwelling of deep undersaturated water favorable for CFC-11 uptake in the subpolar gyres. Even though 90 % of the emissions are in the NH, inter-hemispheric exchange in the atmosphere mixes the CFC-11 concentration quickly. The Southern Ocean is a hotspot of CFC-11 uptake due to cold SSTs, upwelling of CFC-poor deep waters, and strong surface winds conducive to CFC-11 uptake. Upwelling brings undersaturated circumpolar deep water to the surface south of the Antarctic polar front in the Southern Ocean, inducing CFC-11 uptake. These surface waters are transported northward and are ultimately subducted into the interior ocean with intermediate and mode water formation in the sub-Antarctic, accumulating CFC-11 in the interior ocean and preventing it from readily escaping back to the atmosphere in the near future (Figure S3e-h). Due to these processes, more than twice as much CFC-11 is effectively stored in the SH ocean reservoir. The loss of CFC-11 into the global ocean via the air-sea flux is about 8.8 % of the loss in the atmosphere in the 1950s (Table 1). The flux going into the ocean reaches a maximum in the 1980s at 3.6 Gg yr^{-1}. As anthropogenic emissions increase and more CFC-11 accumulates in the atmosphere given its long lifetime, loss in the atmosphere reaches a maximum in the 1990s (at 103.1 Gg yr^{-1}). By the 2010s, the flux going into the ocean is about 1.2 Gg yr^{-1}, or about 1.3 % of the loss occurring in the atmosphere at that time. It is noteworthy that the change in percent loss due to the ocean as compared to the atmosphere decreases by 7.5 % from 1950 to 2020, suggesting a similar fractional increase of the overall CFC-11 lifetime due to the weakening of the ocean uptake.

The calculated global net flux is expected to reverse direction around 2075, with the NH displaying an earlier release of CFC-11 to the atmosphere in 2067, while the SH begins outgassing in 2077 in this model. The reason for the late release of the CFC-11 flux in the SH is due to more CFC-11 being transported into the deeper ocean, which then takes longer to get back to the surface (Figure S3). The maximum flux of CFC-11 out of the ocean occurs in the 2120s, with up to 0.5 Gg yr^{-1} of flux coming back into the atmosphere globally. By the end of 2300, the total flux from the ocean is still 0.2 Gg yr^{-1}. At this point, the loss of CFC-11 in the atmosphere is only 1.4 Gg yr^{-1} given the low atmospheric burden. The effect of the ocean source is counteracting the atmospheric loss by 14 % in the 2290s, suggesting that the CFC-11 lifetime should continue to increase far into the future.

Effect of the ocean on CFC-11 lifetime and emission estimates

The effects of the ocean on CFC-11 lifetimes and therefore on emissions inferred from concentration data are significant. Figure 4a presents lifetimes calculated by taking the model-calculated atmospheric abundances of CFC-11 and dividing by the loss rates in the atmosphere-only and in the atmosphere and ocean together (and similar results for CFC-12 are also given in Figure S4). As expected, when only the atmospheric loss is considered, the lifetime is a constant 55-year as prescribed, but the results including the ocean loss are quite different, at around 50-year in 1950, increasing to about 54-year by 2000 and 60-year by 2250.

To evaluate the effect of the ocean on inferred emissions estimates, we adopt the concentrations from the MITgcm as if they were measured data and infer emissions considering different lifetime assumptions (see Methods section). We then compare these inferred emissions to the emissions used to drive the model. As expected, inferred emission using the dynamic lifetime that includes both the ocean and atmosphere loss (the red curve in Figure 4a) fully recovers the input emissions that drive the MITgcm. Because knowing the exact atmospheric loss rate is not possible in real world, assumed constant atmospheric lifetimes are typically used to estimate emissions. We thus tested using constant 52- 55- and 58-year lifetimes to explore the range of uncertainty in emission estimates. From the 1970s to 1990s, when the ocean uptake was large, inferred emissions using a constant atmospheric lifetime of 52 years provide a closer match to the prescribed emissions that were input to the MITgcm. From 2000 and beyond, when the ocean uptake is small, inferred emissions using a constant 55-year atmospheric lifetime provide a closer match to the prescribed emissions, showing how the large ocean uptake in earlier decades is equivalent to having a shorter atmosphere-only CFC-11 lifetime. Thus, the ocean CFC-11 uptake acts to decrease the overall atmosphere plus ocean lifetime over 1970 – 2000 by about 3 years.

For the key period from 2002 – 2012 to 2014 – 2016, the increase in the input emission for the MITgcm is 11.2 Gg yr^{-1}, while the increase in the inferred emission assuming a constant 55-year lifetime is 11.6 Gg yr^{-1}. This highlights the time-dependent influence of the ocean on atmospheric loss rates of CFC-11. If the ocean's role is ignored, and a constant atmosphere-only lifetime is assumed, then inferring emissions from concentration changes for 2014 – 2016 compared to 2002 – 2012 would overestimate the unexpected emission of CFC-11 by 0.4 ± 0.3 Gg yr^{-1} (assuming a constant lifetime of 55 ± 3 years).

In addition, the atmospheric CFC-11 lifetime has also been shown to be time-dependent rather than constant, largely as a result of the lag time between surface release and stratospheric loss (4). Figure S5 overlays calculated atmosphere-only lifetimes from a suite of chemistry-climate models studied in the SPARC (Stratosphere-troposphere Processes And their Role in Climate) intercomparison. While atmospheric processes alone act to decrease the calculated total lifetime from 1930-2010, ocean processes have the opposite effect. The total lifetime would be best captured by models including both effects, which offset each other to some extent. Changes in atmospheric lifetimes likely explain why our model underestimates the CFC-11 mole fraction after 1990 in Figure 2, since we used a constant atmospheric CFC-11 lifetime throughout those model runs.

Effect of climate change on CFC-11 ocean uptake

The MITgcm simulation under the MPI model's RCP8.5 scenario makes the ocean a weaker reservoir for CFC-11, leading to less uptake in the earlier period and less outgassing in the later period, and climate change affects the timing at certain critical periods. The global ocean starts to release CFC-11 in 2075 under Hist forcing, but the outgassing begins 10 years earlier under the RCP8.5 scenario (Figure 3b). Without climate change, the ocean's effect on the atmospheric concentration of CFC-11 becomes detectable after 2145, compared to 2140 under RCP8.5, suggesting that climate change accelerates the shift towards outgassing CFC-11.

We tested the drivers of these changes using the MITgcm simulations with only certain ocean forcing fields changing under RCP8.5, in order to identify which factors dominate CFC-11 ocean uptake under a changing climate. Zooming in on the period between 2050 and 2090 in Figure 3b, the flux of CFC-11 in the NH under the full RCP8.5 forcing most closely follows that obtained under SST + Qnet (surface heat flux, calculated as latent heat + sensible heat + shortwave + longwave) only forcing. The additional warming of the surface ocean under this forcing leads to more stratified conditions, and reduces the solubility of CFC-11 in seawater, which results in earlier outgassing in the NH. In SST + Qnet only and full RCP8.5 runs, the AMOC decreased similarly (Figure S6c), suggesting that changes in ocean circulation are also playing a major role in weakening uptake, as found in other model studies (13). In the SH, the SST does not increase as much as in the NH, due to the upwelling of deep cold water (25, 26); as such, we find that the SH air-sea CFC-11 flux is mainly affected by changes in salinity as forced by changes in evaporation-precipitation (E-P) and surface restoring of SSS. In particular, increases in net precipitation in the Southern Ocean (Figure S7f) decrease mixed layer depths, leading to weaker ventilation of the intermediate and deep ocean. Thus, more CFC-11 is stored in shallower ocean depths in response to these changes, leading to an earlier outgassing of CFC-11 to the atmosphere in the SH. Note that changes in SSS + E-P forcing do not cause an appreciable weakening of the AMOC (Figure S6c) in this model, unlike changes in SST + Qnet. We emphasize that other models could have different responses to these forcings, and this analysis is intended to be illustrative rather than quantitative.

When the ocean is acting as a sink for CFC-11, the atmosphere has up to 5.0 Gg more CFC-11 under full RCP8.5 forcing than under Hist forcing (Figure S8). In contrast, when the ocean turns into a source of CFC-11, the atmosphere has up to 2.4 Gg less CFC-11 with the full RCP8.5 scenario, which is due to weaker outgassing from the ocean. The combined effect of changes in SST, SSS, and buoyancy fluxes exceeds those in the full RCP8.5 forcing run, because the effects of wind stress on ocean circulation, and of sea ice fraction on air-sea CFC-11 exchange partially counteract the ocean CFC-11 uptake due to thermal and saline changes in this model. Under RCP8.5, there is a poleward intensification of the SH westerly winds (Figure S7), which modifies the ventilation rate and transport of CFC-11 into the ocean (27). In a simulation that isolates the effects of changes in wind stress on the ocean dynamics, there is enhanced ocean uptake, especially over 50 – 60 °S during the early ocean sink period (Figure S3), and the atmosphere has up to 0.8 Gg less CFC-11 compared to the Hist forcing run. When the ocean turns into a source of CFC-11, changes in wind stress forcing can lead to 1.4 Gg more CFC-11 in the atmosphere, due to enhanced equatorward Ekman transport and stronger upwelling in the Southern Ocean (28).

Discussion

Previous work has not explicitly analyzed the effects of the ocean on atmospheric CFC-11 and has generally assumed that the effects of ocean uptake and outgassing can be accounted for by adjusting the uncertainty in atmospheric lifetimes. The results shown here reveal that ocean uptake and outgassing have a much more pronounced effect on our understanding of the lifetime of atmospheric CFC-11 than previously anticipated. The results have small but significant implications for past CFC-11 emission estimates, and key conceptual implications for the future.

Here we summarize our findings on the three primary questions posed in the introduction: First, our model suggests that the ocean's CFC-11 uptake ability varies significantly in time, translating to time-dependence in the total CFC-11 lifetime if the ocean's effect is subsumed into the atmospheric lifetime estimate. This result does not significantly affect calculated ozone depletion or radiative forcing, which often employ prescribed concentrations based on observations. The significance of our work is that knowledge of lifetimes is required to estimate emissions from concentrations and, in turn, to examine emissions sources and consistency with the Montreal Protocol. The calculated 7.5 % increase in lifetime from the 1950s to the 2010s due to weakening ocean uptake affects estimates of CFC-11 emissions by up to 4 Gg yr^{-1}, and it also affects their time dependence, compared to calculations neglecting this effect. We estimate that

the ocean's influence reduces inferred unexpected emission of CFC-11 after 2013 (6, 7) by about 0.4 ± 0.3 Gg yr^{-1} (assuming a constant lifetime of 55±3 years) compared to calculations that neglect the ocean effect. This is because the ocean's weakening sink leads to an increased accumulation of CFC-11 in the atmosphere, which biases estimates of new emissions if the ocean's effect is unaccounted for.

Second, a global net flux coming out of the ocean is projected to begin around 2075, and the release of CFC-11 from this bank implies an accumulating influence on atmospheric CFC-11 abundances that should become detectable in the global average after about 2145, with outgassing up to 0.5 Gg yr^{-1}. Detectable signals could be greatly enhanced and occur sooner if observation sites are located close to ocean upwelling regions, where stronger CFC-11 outgassing can be expected (Figure S3). The ocean ultimately leads to up to a 0.8 ppt increase in the global average atmospheric abundance by 2225. Such observations will signal the return of CFC-11 from the ocean, rather than new production outside the Montreal Protocol at that time.

Finally, an illustrative model projection suggests that climate change will likely make the ocean turn into a source of CFC-11 about 10 years earlier, and will make the effect on atmospheric mixing ratio detectable 5 years earlier according to the scenario presented here. Different models or scenarios could yield differences in detail regarding these findings but are unlikely to alter the general result.

In closing, we note that our results illustrate the importance of the ocean in the new era of the Montreal Protocol in which global anthropogenic productions of ozone depleting substances (ODSs) has dramatically decreased, which means that small sources, sinks, or differences in estimates of lifetimes have now become extremely important because they affect emissions estimates. Atmospheric CFC-11 is not the only ODS taken up to some extent by the ocean. Other gases including for example CFC-12, CCl_4 (carbon tetrachloride) and CH_3CCl_3 (methyl chloroform) are also subject to significant ocean uptake and sequestration, even though it has been demonstrated that CCl_4 and CH_3CCl_3 are not entirely conserved within the ocean (29, 30, 31, 32). Indeed CFC-11 is also not entirely conserved in sufficiently anoxic water characterized by sulfide accumulation (11). Whether this effect could become more significant in future climates depends on where and how deep the ocean sequesters CFC-11, and if sizable regions of anoxic conditions develop in future oceans. Together with changes in ocean temperatures and circulation patterns, these effects could be important in the future for detection of global and regional sources of ODSs. This work highlights the need for the atmospheric chemistry and oceanography communities to further examine these questions involving other ODSs. High-resolution global atmosphere-ocean models, and continued observational programs for global monitoring of ODSs in both the atmosphere and ocean, will be key tools for predicting and detecting these changes in the future.

Materials and Methods

Emission data:

Global CFC-11 emissions up to 2016 (15) are split into NH and SH (33). We adopted a simple constant declining rate of CFC-11 emission from 1995 to 2016 to predict emissions beyond 2016. Emissions in both hemispheres reached zero at around 2100 and were kept zero to the end 2300. A similar treatment is applied for CFC-12 emissions.

Box model equations:

$$\frac{d\,m_{nh}^{a}}{dt} = E_{nh} + F_{nh} - \left(T_{n2s}^{a} + L_{nh}^{a}\right) ¿\, m_{nh}^{a} + T_{s2n}^{a} * m_{sh}^{a} \quad (2)$$

$$\frac{d\,m_{sh}^{a}}{dt} = E_{sh} + F_{sh} - \left(T_{s2n}^{a} + L_{sh}^{a}\right) ¿\, m_{sh}^{a} + T_{n2s}^{a} * m_{nh}^{a} \quad (3)$$

$$\frac{d\,m_{nh}^{t}}{dt} = -F_{nh} - T_{n2s}^{t} * m_{nh}^{t} + T_{s2n}^{t} * m_{sh}^{t} \quad (4)$$

$$\frac{d\,m_{sh}^{t}}{dt} = -F_{sh} - T_{s2n}^{t} * m_{sh}^{t} + T_{n2s}^{t} * m_{nh}^{t} \quad (5)$$

$$\frac{d\,m_{nh}^{d}}{dt} = -\left(T_{nh}^{d2t} + T_{n2s}^{d}\right) * m_{nh}^{d} + T_{nh}^{t2d} * m_{nh}^{t} + T_{s2n}^{d} * m_{sh}^{d} \quad (6)$$

$$\frac{d\,m_{sh}^{d}}{dt} = -\left(T_{sh}^{d2t} + T_{s2n}^{d}\right) * m_{sh}^{d} + T_{sh}^{t2d} * m_{sh}^{t} + T_{n2s}^{d} * m_{nh}^{d} \quad (7)$$

$$F_{nh} = -k\left([CFC]_{nh}^{a} - [CFC]_{nh}^{t}\right) \quad (8)$$

$$F_{sh} = -k\left([CFC]_{sh}^{a} - [CFC]_{sh}^{t}\right) \quad (9)$$

where m indicates mass of CFC-11, L is the CFC-11 atmospheric loss rate, T is the exchange timescale between each box, E is the CFC-11 emission, F is the flux of CFC-11 between the atmosphere and ocean, k is the piston velocity at 10 cm hr^{-1} (34), $[CFC]$ indicates the concentration in the atmosphere and mixed layer boxes. Superscripts indicate layers and subscripts indicate the hemisphere. Table S1 shows a description of each term as well as the numerical values associated with each parameter.

MITgcm model:

Emission, atmospheric loss rate, and the atmosphere inter-hemispheric exchange timescale for CFC-11 in the MITgcm runs are the same as used in the box model setup. The CFC-11 air-sea flux equation is the same as shown in equations 8 – 9 (35), except that each term is calculated locally and dynamically given changes in the ocean forcing. Transport of CFC-11 within the ocean is done by the MITgcm. The MITgcm ocean model used here has 2.8° × 2.8° horizontal resolution and 15 vertical layers down to 5000 m. This is a fairly coarse resolution, but appears sufficient to provide a first order estimate of CFC-11 uptake in the past based on Figure 2, and hence is used to estimate the long-term future. A mesoscale eddy parameterization (36) is used with an eddy diffusivity set to 1000 m^2 s^{-1}. Convective adjustment is applied to statically unstable water columns, and background vertical diffusivity is set to 5×10^{-5} m^2 s^{-1}. Improved resolution and adjustments in ocean model parameters have been shown to impact details of CFCs storage within the ocean (13, 37), but we would not expect such changes to alter our qualitative results. Figure S6 shows the resulting residual mean meridional overturning circulation in the Atlantic Ocean, which appears reasonable.

MITgcm forcing fields:
The MITgcm is forced by monthly net E-P-R and Qnet climatologies (38). In addition, SST and SSS in the upper 50 m ocean layer are restored to a monthly climatology based on survey data taken from 1950 to 1990 (39, 40), with restoring timescales of 60 and 90 days respectively. Wind stress and wind speed climatologies over this period are from the European Centre for Medium-Range Weather Forecasts (ECMWF; 41, 42). Wind speed is decoupled from the wind stress in this setup and is only used to calculate the piston velocity for CFC-11 air-sea flux (i.e., it has no impact on ocean dynamics, in contrast with applied wind stress). The monthly sea ice concentration climatology (43, 44), like the surface wind speed, is only used in the calculation of CFC uptake; note our MITgcm setup does not include a prognostic sea ice model. The ocean was subject to 5900 years of spinup with the above climatology to produce an equilibrium state, followed by runs with CFC-11 from 1930 to 2300.

MITgcm RCP8.5 setup:
In this simulation the ocean dynamical model is spun up to equilibrium in the same way as the Hist run. Modified forcing fields using RCP8.5 output from MPI-ESM-LR (18, 19) during the transient simulation from 1930-2300 were constructed as follows. First we coarse-grained the output from MPI-ESM-LR using a nearest neighbor algorithm to MITgcm's 2.8° × 2.8° resolution, and constructed a base period from 1850 to 1930 (using MPI-ESM-LR's historical simulation). Monthly anomalies from 1930 to 2300 compared to the base period were then added to the MITgcm Hist forcing discussed above (anomalies were imposed beginning in the early 20th century to avoid any abrupt changes in forcing fields that might cause unphysical changes in ocean circulation). Figure S7 shows the spatial patterns of the RCP8.5 anomalies for all the forcing variables nudged in MITgcm. Unlike in the Hist simulation, in the RCP8.5 simulation the ocean circulation and air-sea gas exchange piston velocity both evolve over time. AMOC strength in the MITgcm RCP8.5 run decreases by 60 % from 1930 – 2000 to 2200 – 2300 (Figure S6), comparable to a 56 % decrease obtained in the MPI-ESM-LR.

Top-down inferred emission based on the MITgcm output:
We inferred the emission and the atmospheric lifetime from the MITgcm output of the CFC-11 (and CFC-12) inventory by:

$$E_{inf} = \frac{dm}{dt} + \frac{m}{\tau} \quad (10)$$

$$\tau_{atm} = \frac{m}{L^a_{nh} + L^a_{sh}} \quad (11)$$

$$\tau_{atm+ocn} = \frac{m}{L^a_{nh} + L^a_{sh} + F_{nh} + F_{sh}} \quad (12)$$

where E_{inf} is the inferred emission, m is the mass of CFC-11 (and CFC-12) as calculated from the MITgcm, $\frac{dm}{dt}$ is the tendency of the CFC-11 (and CFC-12) inventories. τ_{atm} is the inferred CFC-11 (and CFC-12) lifetime only considering the atmospheric loss, and $\tau_{atm+ocn}$ is the total lifetime considering both the atmospheric loss and the bi-directional flux from the ocean. τ in equation 10 is replaced with inferred lifetimes from equations 11 – 12 as well as assumed constant 52- and 58-year lifetime for the inferred emission estimates in Figure 4b for CFC-11 (assumed constant 90- and 100-year lifetime in Figure S4b for CFC-12).

Data availability:

The MITgcm output under different forcing runs and the code used here are available publicly on Zenodo (DOI: 10.5281/zenodo.4435502).

Acknowledgments

The authors appreciate the CFCs data provided by Matthew Rigby. P.W., S.S., and M.L. gratefully acknowledge support by a grant from VoLo foundation; S.S. and D.W.T. appreciate support under NSF-1848863. A.R.B. appreciates support from Simons Foundation grant 622065. T.D. acknowledges NSF OCE-1948955. The authors are grateful for feedback from Ray Weiss. The authors also thank the two anonymous reviewers for their comments.

References

1. S. Solomon, Stratospheric ozone depletion: A review of concepts and history. *Rev. Geophys.* **37**, 275–316 (1999).
2. S. Solomon, *et al.*, Emergence of healing in the Antarctic ozone layer. *Science (80-.).* **353**, 269–274 (2016).
3. WMO, “Scientific Assessment of Ozone Depletion: 2002” in Global Ozone Research and Monitoring Project – Report No. 47. (World Meteorological Organization, Geneva Switzerland, 2003).
4. M. P. Chipperfield, *et al.*, Journal of Geophysical Research : Atmospheres. *J. Geophys. Res. Atmos.* **119**, 2555–2573 (2014).
5. M. Lickley, *et al.*, Quantifying contributions of chlorofluorocarbon banks to emissions and impacts on the ozone layer and climate. *Nat. Commun.* **11** (2020).
6. S. A. Montzka, *et al.*, An unexpected and persistent increase in global emissions of ozone-depleting CFC-11. *Nature* **557**, 413–417 (2018).
7. M. Rigby, *et al.*, Increase in CFC-11 emissions from eastern China based on atmospheric observations. *Nature* **569**, 546–550 (2019).
8. M. J. Warner, R. F. Weiss, Solubilities of chlorofluorocarbons 11 and 12 in water and seawater. *Deep Sea Res. Part A, Oceanogr. Res. Pap.* **32**, 1485–1497 (1985).
9. D. A. Willey, *et al.*, Global oceanic chlorofluorocarbon inventory. *Geophys. Res. Lett.* **31**

(2004).
10. T. DeVries, M. Holzer, Radiocarbon and Helium Isotope Constraints on Deep Ocean Ventilation and Mantle-3He Sources. *J. Geophys. Res. Ocean.* **124**, 3036–3057 (2019).
11. J. L. Bullister, B. -S Lee, Chlorofluorocarbon-11 removal in anoxic marine waters. *Geophys. Res. Lett.* **22**, 1893–1896 (1995).
12. T. Ito, J. Marshall, M. Follows, What controls the uptake of transient tracers in the Southern Ocean? *Global Biogeochem. Cycles* **18**, 1–17 (2004).
13. A. Romanou, J. Marshall, M. Kelley, J. Scott, Role of the ocean's AMOC in setting the uptake efficiency of transient tracers. *Geophys. Res. Lett.* **44**, 5590–5598 (2017).
14. A. Golombek, R. G. Prinn, A global three-dimensional model of the circulation and chemistry of CFCl3, CF2Cl2, CH3CCl3, CCl4, and N2O. *J. Geophys. Res.* **91**, 3985 (1986).
15. A. Engel, M. Rigby et al., "Update on Ozone-Depleting Substances (ODSs) and other gases of interest to the Montreal Protocol" in Scientific Assessment of Ozone Depletion: 2018, Global Ozone Research and Monitoring Project. Report No. 58. (World Meteorological Organization, 2019), pp. 1.1–1.66.
16. J. Marshall, A. Adcroft, C. Hill, L. Perelman, C. Heisey, A finite-volume, incompressible navier stokes model for, studies of the ocean on parallel computers. *J. Geophys. Res. C Ocean.* **102**, 5753–5766 (1997).
17. J. Marshall, C. Hill, L. Perelman, A. Adcroft, Hydrostatic, quasi-hydrostatic, and nonhydrostatic ocean modeling. *J. Geophys. Res. C Ocean.* **102**, 5733–5752 (1997).
18. J. H. Jungclaus, *et al.*, Characteristics of the ocean simulations in the Max Planck Institute Ocean Model (MPIOM) the ocean component of the MPI-Earth system model. *J. Adv. Model. Earth Syst.* **5**, 422–446 (2013).
19. M. A. Giorgetta, *et al.*, Climate and carbon cycle changes from 1850 to 2100 in MPI-ESM simulations for the Coupled Model Intercomparison Project phase 5. *J. Adv. Model. Earth Syst.* **5**, 572–597 (2013).
20. Y. Kostov, *et al.*, Fast and slow responses of Southern Ocean sea surface temperature to SAM in coupled climate models. *Clim. Dyn.* **48**, 1595–1609 (2017).
21. J. L. Bullister, Data from "Atmospheric Histories (1765-2015) for CFC-11, CFC-12, CFC-113, CCl4, SF6 and N2O (NCEI Accession 0164584)." NOAA National Centers for Environmental Information. Available at https://doi.org/10.3334/cdiac/otg.cfc_atm_hist_2015. Deposited 4 August 2017.
22. J. C. Dutay, *et al.*, Evaluation of ocean model ventilation with CFC-11: Comparison of 13 global ocean models. *Ocean Model.* **4**, 89–120 (2002).
23. R. A. Fine, K. A. Maillet, K. F. Sullivan, D. Willey, Circulation and Ventilation flux of the Pacific Ocean. *J. Geophys. Res. Ocean.* **106**, 22159–22178 (2001).
24. R. G. Prinn, *et al.*, History of chemically and radiatively important atmospheric gases from the Advanced Global Atmospheric Gases Experiment (AGAGE). *Earth Syst. Sci. Data* **10**, 985–1018 (2018).
25. K. C. Armour, J. Marshall, J. R. Scott, A. Donohoe, E. R. Newsom, Southern Ocean warming delayed by circumpolar upwelling and equatorward transport. *Nat. Geosci.* **9**, 549–554 (2016).
26. J. Marshall, *et al.*, The ocean's role in the transient response of climate to abrupt greenhouse gas forcing. *Clim. Dyn.* **44**, 2287–2299 (2015).
27. D. W. Waugh, Changes in the ventilation of the southern oceans. *Philos. Trans. R. Soc. A Math. Phys. Eng. Sci.* **372**, 568–571 (2014).
28. N. S. Lovenduski, N. Gruber, Impact of the Southern Annular Mode on Southern Ocean circulation and biology. *Geophys. Res. Lett.* **32**, 1–4 (2005).
29. O. Huhn, W. Roether, P. Beining, H. Rose, Validity limits of carbon tetrachloride as an ocean tracer. *Deep Sea Res. Part I Oceanogr. Res. Pap.* **48**, 2025–2049 (2001).
30. R. G. Prinn, *et al.*, Evidence for substantial variations of atmospheric hydroxyl radicals in the past two decades. *Science (80-.).* **292**, 1882–1888 (2001).
31. P. O. Wennberg, S. Peacock, J. T. Randerson, R. Bleck, Recent changes in the air-sea gas exchange of methyl choloroform. *Geophys. Res. Lett.* **31**, 3–6 (2004).

32. D. W. R. Wallace, P. Beining, A. Putzka, Carbon tetrachloride and chlorofluorocarbons in the South Atlantic Ocean, 19°S. *J. Geophys. Res. Ocean.* **99**, 7803–7819 (1994).
33. M. Rigby, *et al.*, Re-evaluation of the lifetimes of the major CFCs and CH3CCl3 using atmospheric trends. *Atmos. Chem. Phys.* **13**, 2691–2702 (2013).
34. M. H. England, V. Garcon, J. F. Minster, Chlorofluorocarbon uptake in a world ocean model 1. Sensitivity to the surface gas forcing. *J. Geophys. Res.* **99** (1994).
35. R. Wanninkhof, Relationship between wind speed and gas exchange over the ocean. *J. Geophys. Res.* **97**, 7373–7382 (1992).
36. P. R. Gent, J. C. Mcwilliams, Isopycnal Mixing in Ocean Circulation Models. *J. Phys. Oceanogr.* **20**, 150–155 (1990).
37. J.-O. Beismann, R. Redler, Model simulations of CFC uptake in North Atlantic Deep Water: Effects of parameterizations and grid resolution. *J. Geophys. Res.* **108**, 1–16 (2003).
38. S. Jiang, P. H. Stone, P. Malanotte-Rizzoli, An assessment of the Geophysical Fluid Dynamics Laboratory ocean model with coarse resolution: Annual-mean climatology. *J. Geophys. Res. Ocean.* **104**, 25623–25645 (1999).
39. S. Levitus, R. Burgett, T. P. Boyer, “World ocean atlas 1994, Vol. 3: salinity” in NOAA Atlas NESDIS (U.S. Gov. Printing Office, Wash., D.C., 1994).
40. S. Levitus, T. P. Boyer, “World ocean atlas 1994, Vol. 4: temperature” in NOAA Atlas NESDIS (U.S. Gov. Printing Office, Wash., D.C., 1994).
41. K. E. Trenberth, W. G. Large, J. G. Olson, The Mean Annual Cycle in Global Ocean Wind Stress. *J. Phys. Oceanogr.* **20** (1990).
42. K. E. Trenberth, J. G. Olson, W. G. Large, A Global Ocean Wind Stress Climatology Based on ECMWF Analyses. *NCAR Tech. note* (1989) https:/doi.org/10.5065/D6ST7MR9.
43. W. Chapman and National Center for Atmospheric Research Staff (Eds), Data from “The Climate Data Guide: Walsh and Chapman Northern Hemisphere Sea Ice.” Available at https://climatedataguide.ucar.edu/climate-data/walsh-and-chapman-northern-hemisphere-sea-ice.
44. H. J. Zwally, *et al.*, “Antarctic Sea Ice, 1973-1976: Satellite Passive-Microwave Observations” in NASA SP-459 (Washington, D.C.: National Aeronautics and Space Administration, 1983).

Figures and Tables

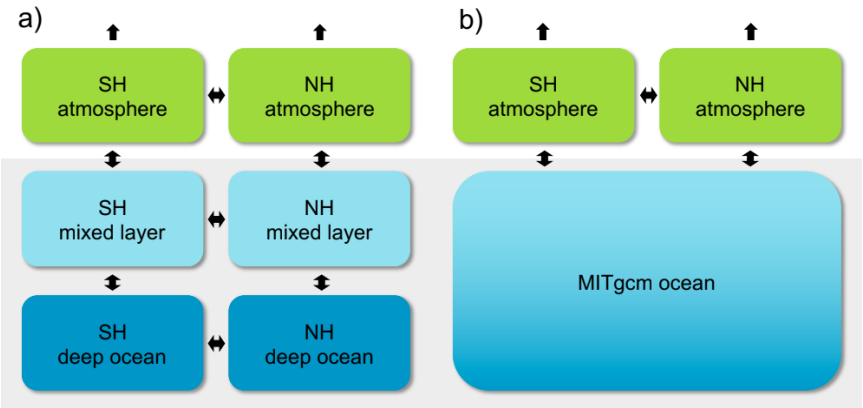

Figure 1. Schematic diagrams showing a) the box model; and b) the MITgcm setup. The box model has three layers that represent the atmosphere, ocean mixed layer and deep ocean. Each layer has two boxes that indicate the NH and the SH. The MITgcm setup replaces the four ocean boxes with the MITgcm ocean but keeps the atmospheric boxes unchanged. One-way arrows indicate CFC-11 atmospheric loss; two-way arrows indicate CFC-11 transport into/out of the box.

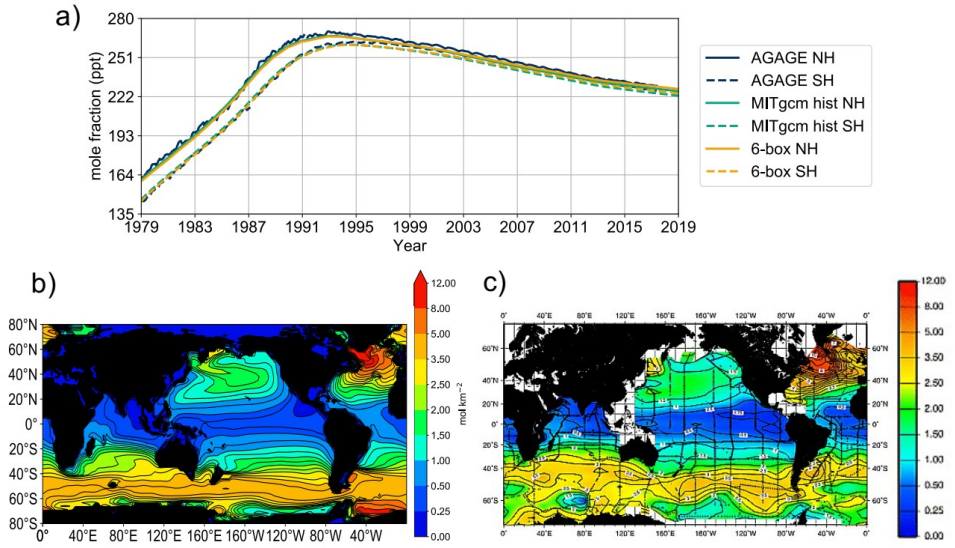

Figure 2. a) Model validation of CFC-11 atmospheric abundances compared to CFC-11 atmospheric surface data (14); b) the MITgcm ocean column integrated CFC-11 under Hist run; and c) observations of ocean column integrated CFC-11 (9). Panels b and c both show the CFC-11 inventories in the year 1994, and are in the same units of mol km^{-2}.

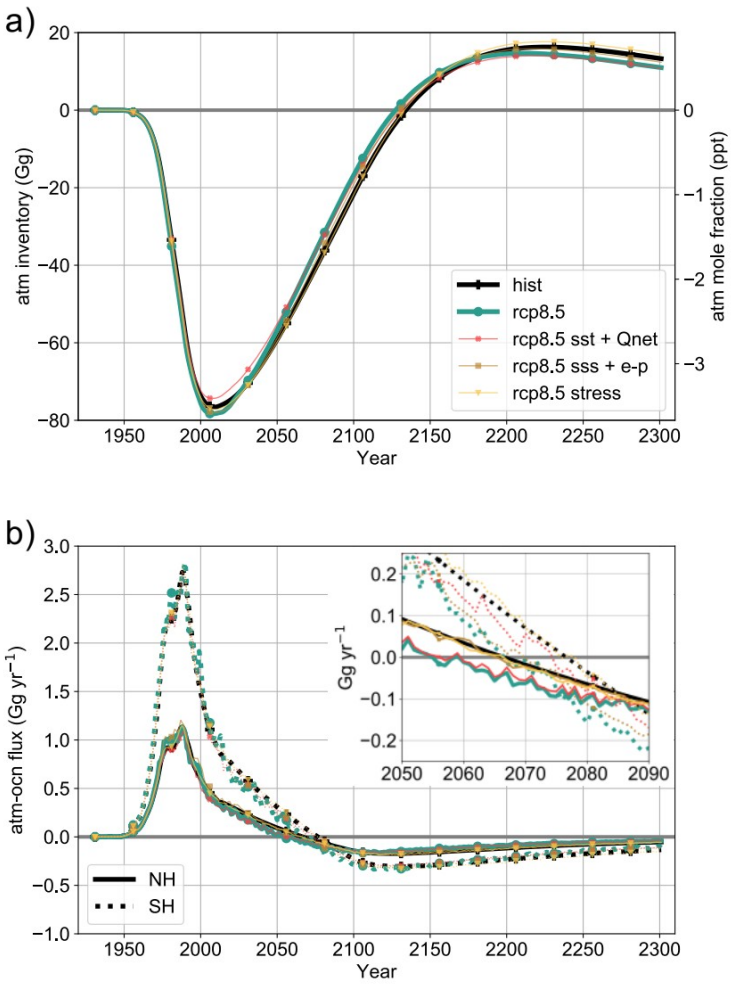

Figure 3. a) Atmospheric CFC-11 inventory (left axis) and abundance (right axis) for different ocean forcing tests (different colors and markers) in the MITgcm minus the atmosphere under no ocean run; results are shown both for the Hist and RCP8.5 runs. The differences between sea ice only and the wind speed only forcing results are nondifferentiable from the result using historical forcing, especially after 2100, and are omitted from this figure; b) MITgcm hemispherically-integrated CFC-11 air-sea flux under different ocean forcings. Positive values indicate fluxes going from the atmosphere to the ocean. Solid lines are the NH integrated flux and dashed lines are the SH integrated flux. Bottom panel is zoomed in between 2050 and 2090, when the flux changes sign.

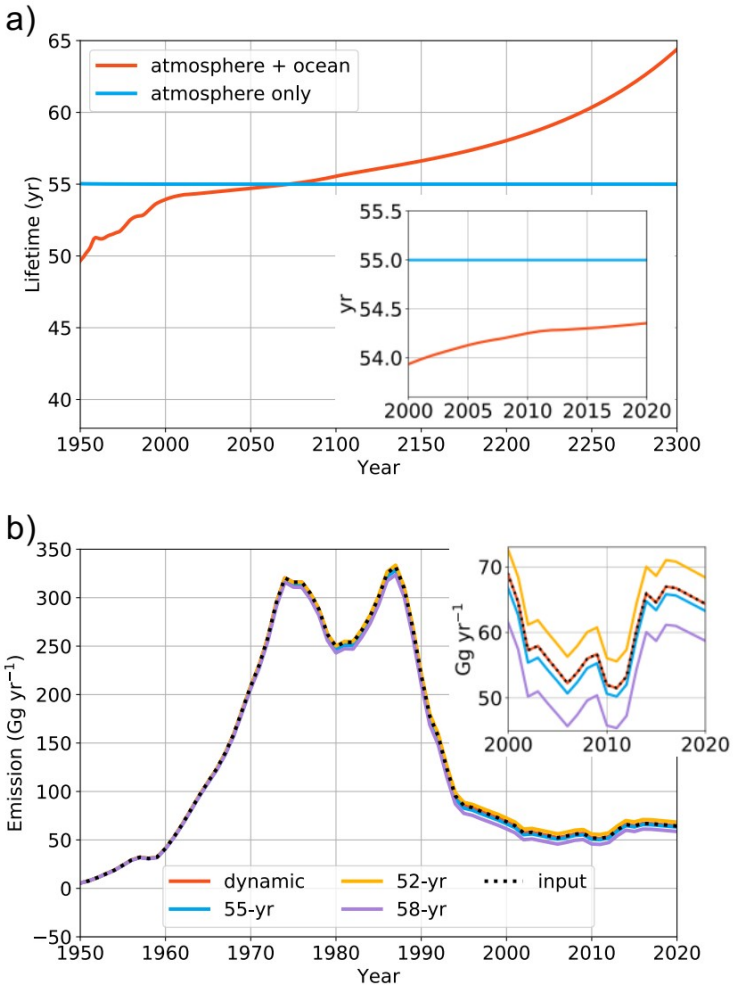

Figure 4. a) Lifetime of atmospheric CFC-11 in the model calculated by including only atmospheric losses (blue line) and including both atmosphere and ocean (red line); b) Comparison between emissions prescribed in the MITgcm runs to those inferred by treating the model calculated concentrations as data and ignoring the effect of the ocean on the lifetime. Black dashed line shows the emission input to the run. We use a 1-box model to do a top-down estimate of the emission (see Methods) given the CFC-11 concentrations that are output from the MITgcm using: a dynamic CFC-11 atmospheric-ocean lifetime (same as the red line in panel a); constant 55-year atmosphere-only lifetime (same as the blue line in panel a); and constant 52- and 58-year lifetimes to test the sensitivity of the inferred emissions. Inferred emission is shown from 1950 to 2020; emission after 2020 approaches zero linearly.

Table 1. Calculated loss of CFC-11 in the atmosphere assuming a constant 55-year lifetime, loss of CFC-11 to the ocean as air-sea flux (positive values indicate a flux of CFC-11 from the atmosphere to the ocean), and relative loss in the ocean compared to that in the atmosphere from the MITgcm simulations. Values for several decades around the period of maximum loss in the atmosphere (1990s), the period of maximum flux of CFC-11 from the ocean to the atmosphere (2120s) and the outgassing late in the 23rd century are shown in the table. Error bars indicate ± 1 standard deviation associated with the decadal average. Loss rates in the 1930s and 1940s are very small compared to the error bars, and are not shown.

Time	Atmosphere loss (Gg yr^{-1})	Ocean loss (Gg yr^{-1})	Ocean/atmosphere loss (%)
1951 – 1960	2.3 ± 1.4	0.2 ± 0.1	8.8 ± 1.1
1961 – 1970	14.2 ± 6.5	1.0 ± 0.4	7.1 ± 0.3
1971 – 1980	50.4 ± 12.7	2.8 ± 0.4	5.7 ± 0.7
1981 – 1990	88.3 ± 10.5	3.6 ± 0.2	4.1 ± 0.3
1991 – 2000	103.1 ± 1.2	2.6 ± 0.4	2.5 ± 0.4
2001 – 2010	96.6 ± 2.3	1.6 ± 0.2	1.6 ± 0.2
2011 – 2020	90.0 ± 1.4	1.2 ± 0.1	1.3 ± 0.0
…	…	…	…
2101 – 2110	35.0 ± 1.8	-0.4 ± 0.0	-1.2 ± 0.1
2111 – 2120	29.3 ± 1.5	-0.5 ± 0.0	-1.6 ± 0.1
2121 – 2130	24.5 ± 1.3	-0.5 ± 0.0	-2.0 ± 0.1
2131 – 2140	20.5 ± 1.0	-0.5 ± 0.0	-2.3 ± 0.1
2141 – 2150	17.2 ± 0.9	-0.5 ± 0.0	-2.7 ± 0.1
…	…	…	…
2281 – 2290	1.6 ± 0.1	-0.2 ± 0.0	-12.7 ± 0.4
2291 – 2300	1.4 ± 0.1	-0.2 ± 0.0	-14.0 ± 0.4

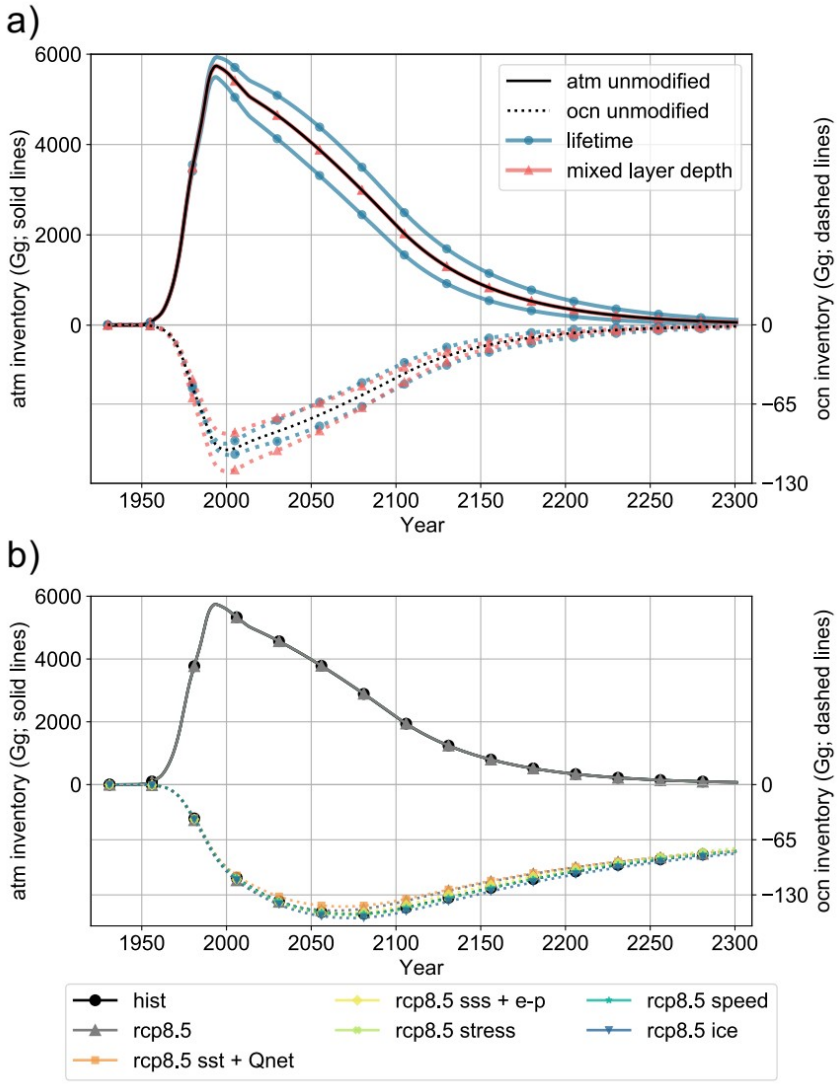

Figure S1. a) Box model CFC-11 inventories for the atmosphere (left axis and solid lines) and the ocean (right axis and dashed lines). Black lines indicate CFC-11 inventories with unmodified parameters as in Table S1, and colored lines display ± 15 % changes of these associated parameters (only the results from most sensitive parameters are shown in the figure). b) MITgcm CFC-11 inventories under additional ocean forcing runs. In both panels, the ocean inventory is shown inversed in sign to facilitate comparison.

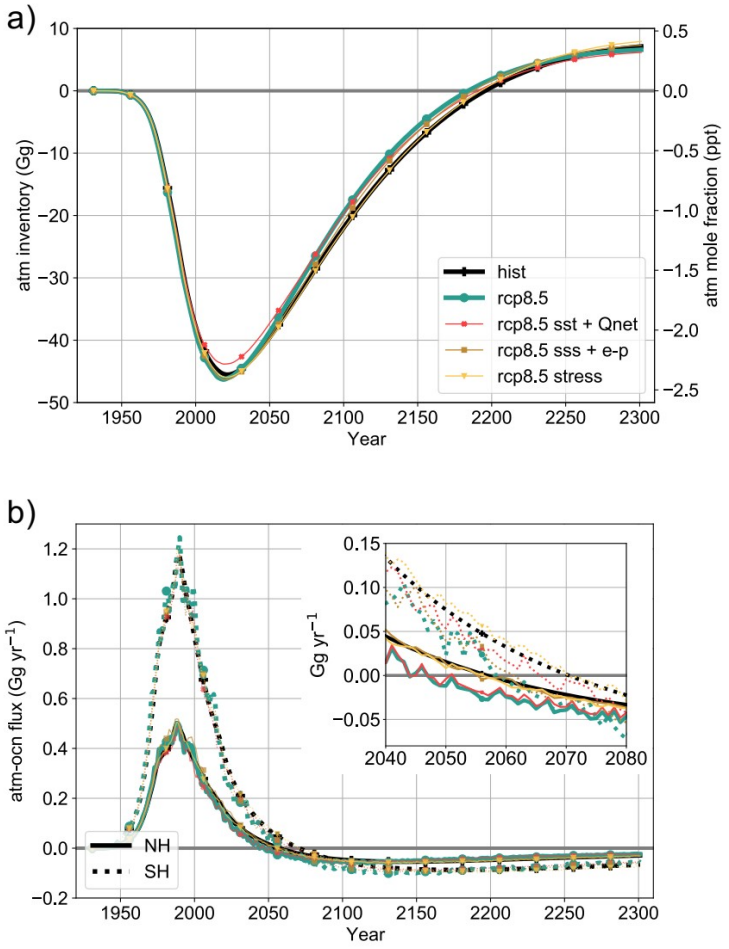

Figure S2. Similar to Figure 3, but for CFC-12.

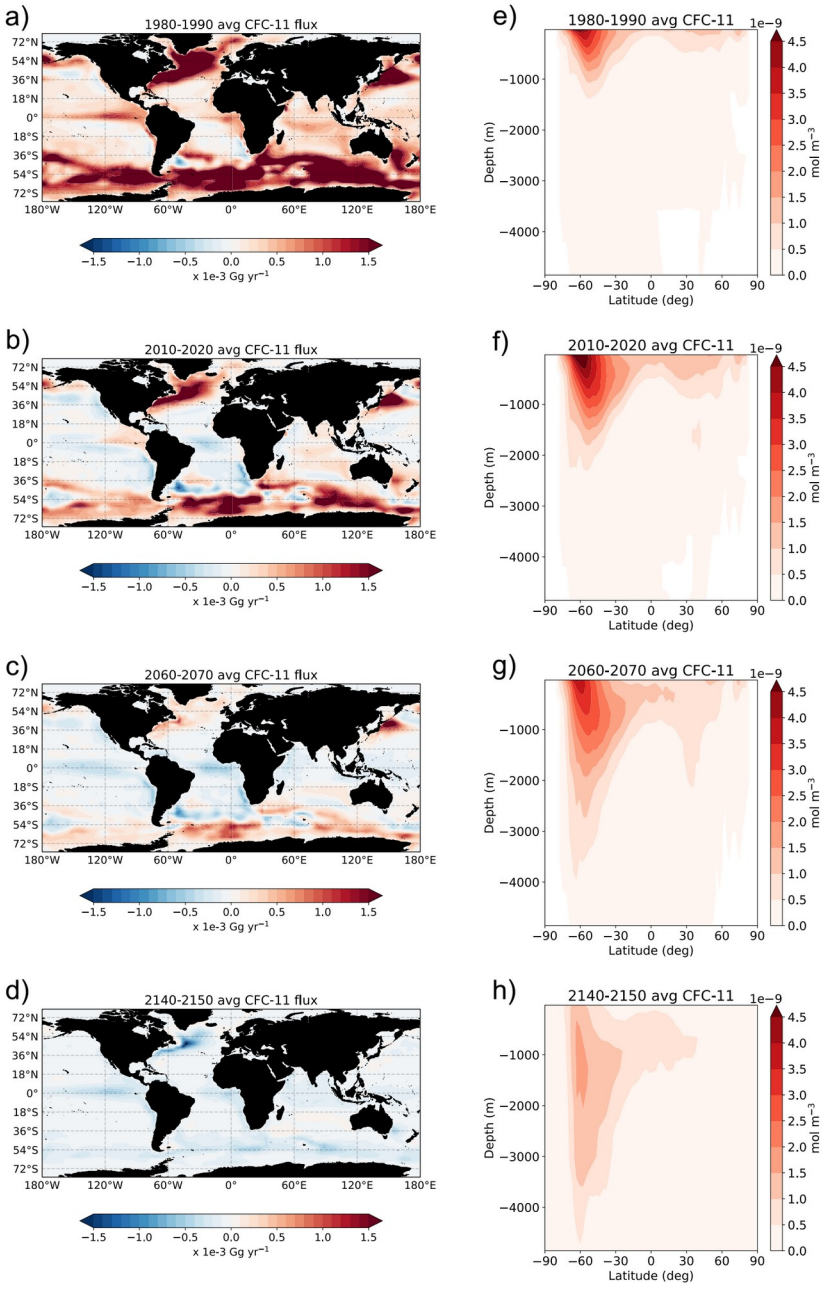

Figure S3. a – d) Decadal averages of CFC-11 air-sea flux (area integrated) for different time periods in the MITgcm Hist run (positive indicate fluxes going into the ocean); e – h) Zonal mean CFC-11 concentration in the ocean for the same averaging periods shown on the left.

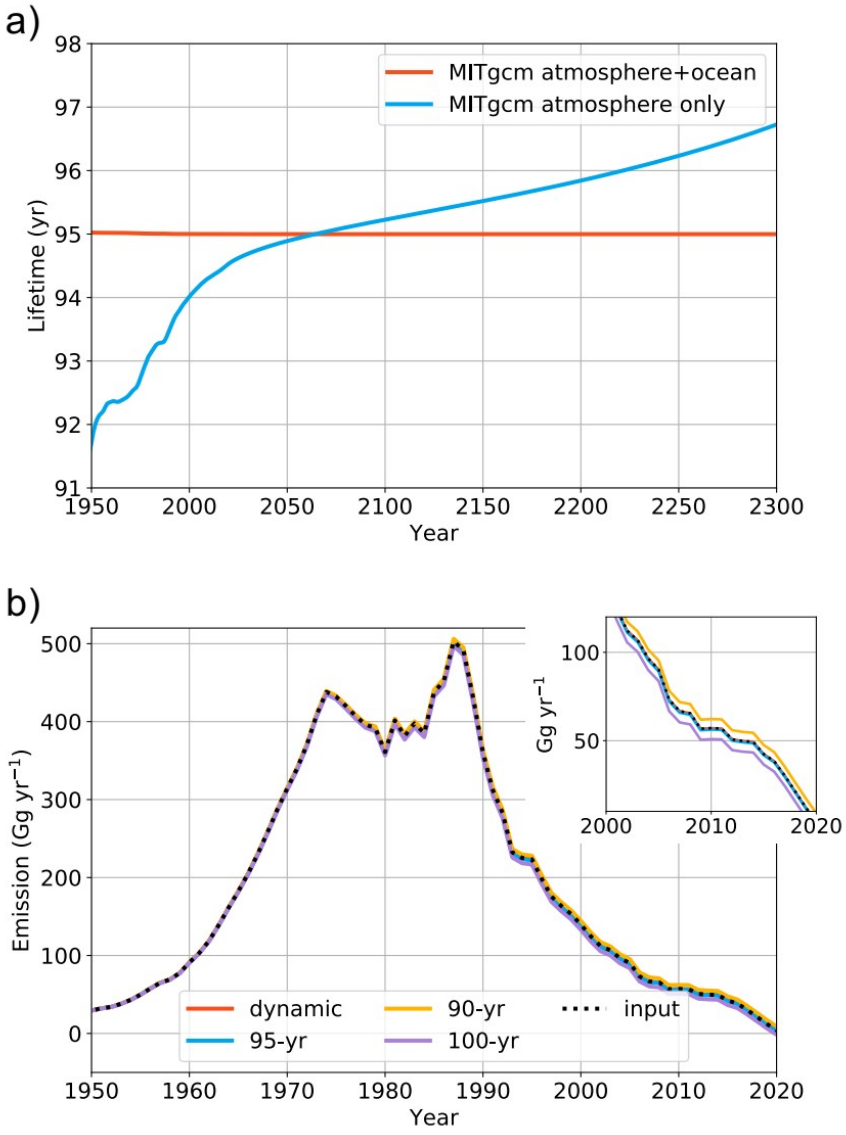

Figure S4. Similar to Figure 4, but for CFC-12.

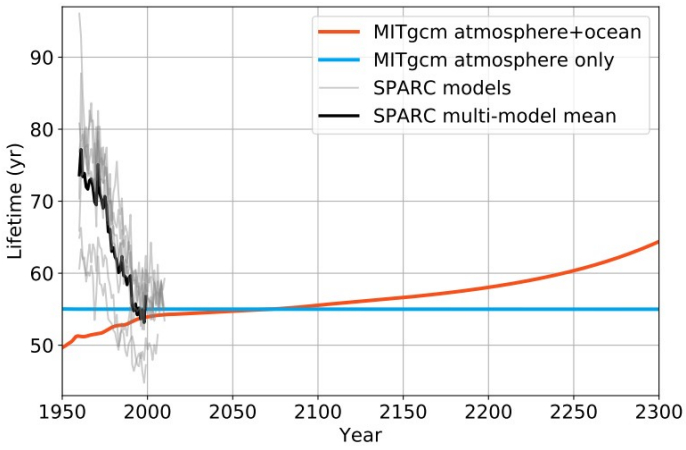

Figure S5. Same as Figure 3, except that atmosphere-only CFC-11 lifetime calculated from SPARC chemistry-climate models are overlaid for comparison. Thin gray lines are calculated time-dependent atmosphere-only lifetimes from the SPARC models from 1960 to 2010, while the heavy black line is the SPARC multi-model mean.

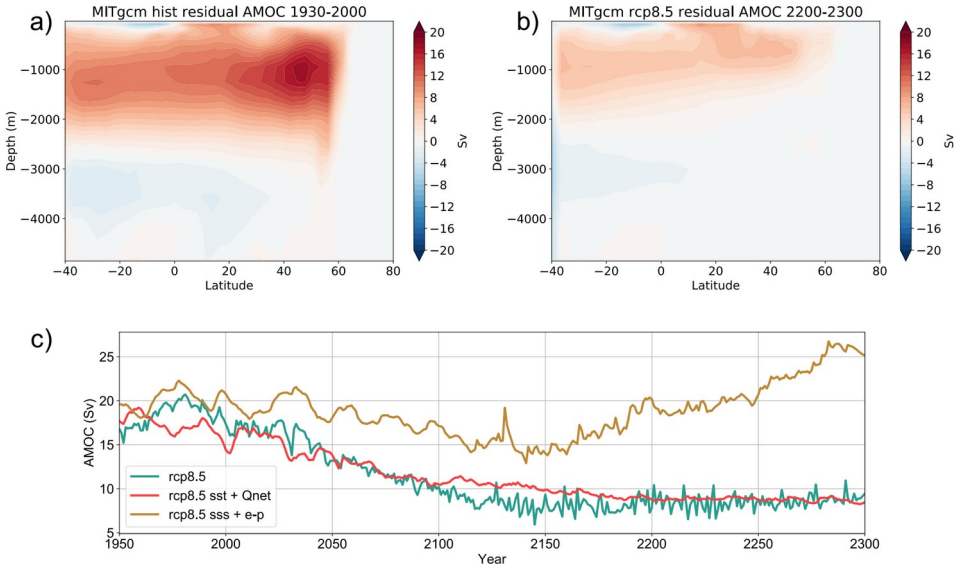

Figure S6. a) Zonal mean residual AMOC under Hist run averaged in 1930 – 2000; b) Zonal mean residual AMOC under RCP8.5 run averaged in 2200 – 2300; c) Time series of AMOC strength (maximum between 20 – 50 °N) under full RCP8.5, SST + Qnet only and SSS + E-P only. Under full RCP8.5, AMOC in the MITgcm has decreased by 60 % from 1930 – 2000 to 2200 – 2300. This percent decrease is comparable to MPI-ESM-LR, which shows a 56 % decrease during the same period, except that the AMOC climatology in MPI-ESM-LR started at a higher value than the MITgcm at the beginning of 1930.

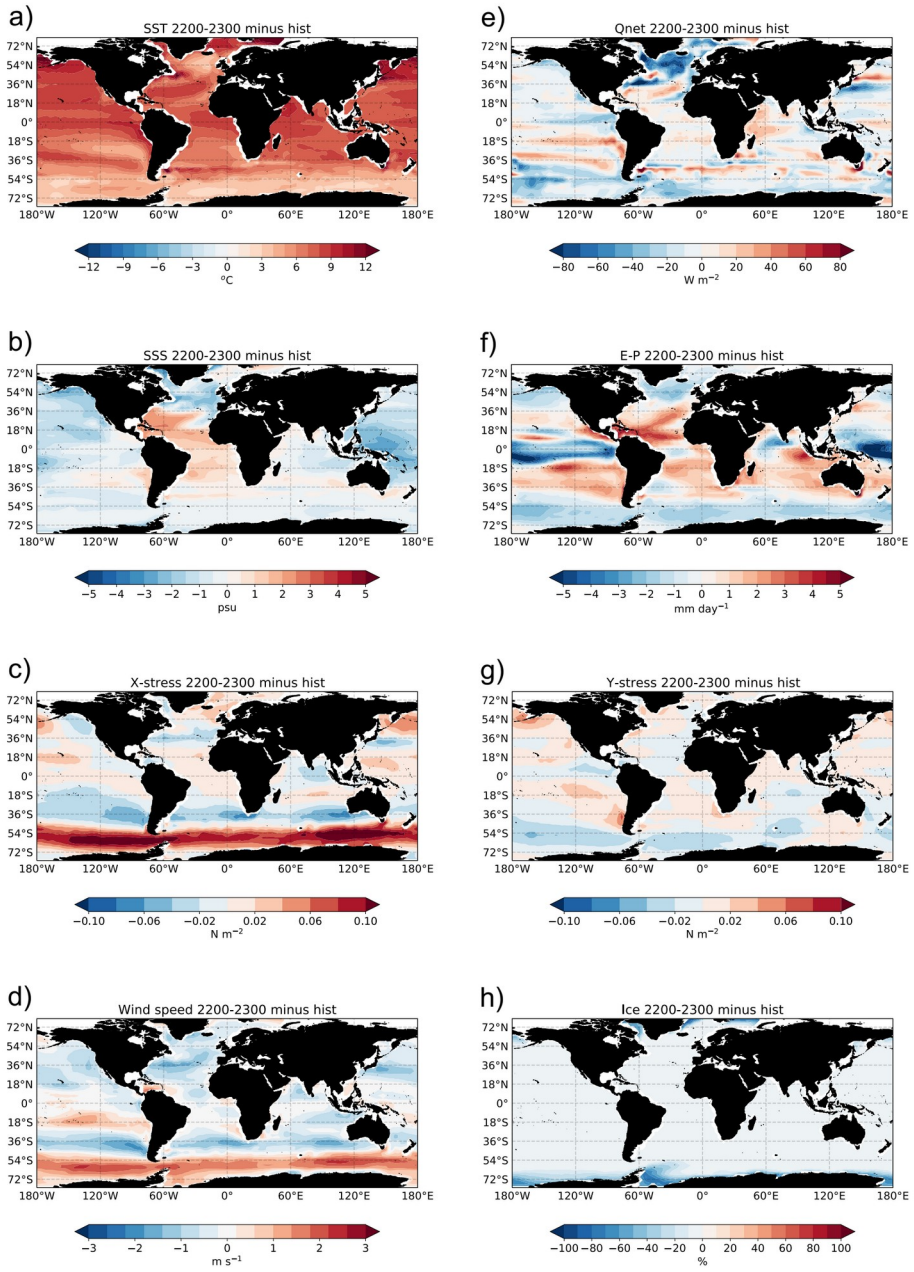

Figure S7. Anomaly maps of all the forcing fields from the MPI-ESM-LR RCP8.5 scenario. The maps indicate averages of the last 100 years (2200 – 2300) minus the base period (1850 – 1930).

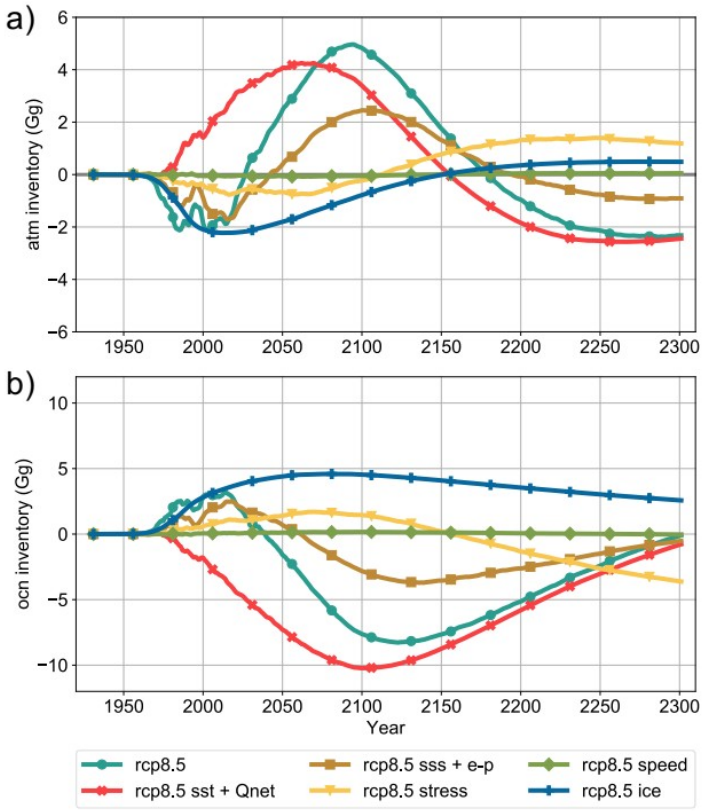

Figure S8. CFC-11 inventory difference between each RCP8.5 forcing run and Hist forcing run for a) atmosphere inventories; and b) ocean inventories.

Table S1. A list of parameters and variables used in the box model.

Name	Value Used	Description
m^a_{nh}, m^a_{sh}	Calculated in the model	CFC-11 mass in the atmospheric boxes, subscript indicates the NH and SH.
m^t_{nh}, m^t_{sh}	Calculated in the model	CFC-11 mass in the mixed layer boxes, subscript indicates the NH and SH.
m^d_{nh}, m^d_{sh}	Calculated in the model	CFC-11 mass in the deep ocean boxes, subscript indicates the NH and SH.
F_{nh}, F_{sh}	Calculated in the model	CFC-11 air-sea flux.
E_{nh}, E_{sh}	Discussed in the text	CFC-11 emission in the NH and SH.
L	1/55 yr^{-1}	CFC-11 atmospheric loss rate.
T^a_{n2s}, T^a_{s2n}	1/1.3 yr^{-1}	Atmospheric exchange rate between the NH and SH.
T^t_{n2s}, T^t_{s2n}	1/50 yr^{-1}	Mixed layer exchange rate between the NH and SH.
T^d_{n2s}, T^d_{s2n}	1/100 yr^{-1}	Deep ocean exchange rate between the NH and SH.
T^{t2d}_{nh}, T^{t2d}_{sh}	1/3 yr^{-1}	Mixed layer to deep ocean exchange rate in the NH and SH.
T^{d2t}_{nh}, T^{d2t}_{sh}	1/5 yr^{-1}	Deep ocean to mixed layer exchange rate in the NH and SH.
k	10 cm hr^{-1}	Piston velocity.
H^a	13 km	Atmosphere height.
A^a	5.1e+14 m^2	Atmospheric total surface area.
H^t	150 m	Mixed layer depth.
A^t	3.1e+14 m^2	Ocean total surface area (assume 15% sea ice)